UCRL-TR-210492

LAWRENCE
LIVERMORE
NATIONAL
LABORATORY

Studies of the Pulse-Line Accelerator Using a Circuit Model

A. Friedman

March 14, 2005

Disclaimer

This document was prepared as an account of work sponsored by an agency of the United States Government. Neither the United States Government nor the University of California nor any of their employees, makes any warranty, express or implied, or assumes any legal liability or responsibility for the accuracy, completeness, or usefulness of any information, apparatus, product, or process disclosed, or represents that its use would not infringe privately owned rights. Reference herein to any specific commercial product, process, or service by trade name, trademark, manufacturer, or otherwise, does not necessarily constitute or imply its endorsement, recommendation, or favoring by the United States Government or the University of California. The views and opinions of authors expressed herein do not necessarily state or reflect those of the United States Government or the University of California, and shall not be used for advertising or product endorsement purposes.

This work was performed under the auspices of the U.S. Department of Energy by University of California, Lawrence Livermore National Laboratory under Contract W-7405-Eng-48.

Studies of the pulse-line accelerator using a circuit model*

Alex Friedman

March 8, 2005

This note describes a simple model developed to explore some of the properties of the pulse-line ion accelerator [1], here represented as a series of lumped elements, in the general parameter regime for the "NDCX-1d" experiments. The goals of this modeling are: to understand the evolution of various possible input pulses in the presence of dispersive effects and imperfect termination of the line; to examine scenarios for beam acceleration; and to explore the effects of "beam loading", that is, changes to the voltages along the helical line that result from the interaction of the beam's return current with the "circuitry" of that line.

In Section 1 below, the model is described and the method of solution outlined; in Section 2, a low-current example of beam acceleration is presented; in Section 3, runs are presented showing the development of beam loading-induced voltages as model pulses are followed; in section 4, the modeling of a higher-current beam under acceleration is presented, and the effects of beam loading quantified; and in section 5, a brief summary of complementary efforts and of plans to extend the modeling is presented.

1 Description of the Model

The model employed in these studies consists of an L-C network terminated by a resistor. This model affords pulse propagation with minimal dispersion for wavelengths long compared to the spacing of the nodes at which the voltage is evaluated. In the runs presented here, the node spacing corresponds to the axial distance s separating neighboring turns of the helix. A more realistic model would incorporate dispersion associated with the mutual inductances and capacitances at all separations; indeed, the actual code includes a full set of mutual inductances and (temporarily, for simplicity) only the nearest-neighbor "shunt" capacitances (in parallel with the inductors). These elements were not employed in the runs described in this note. The model is depicted in Fig. 1.

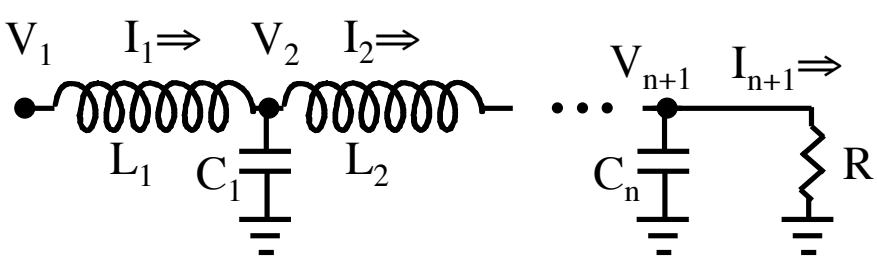

Figure 1: Schematic of the circuit model. Drive voltage $V_1(t)$ is applied at node 1; source terms associated with the return current induced in the helix by the beam are not shown.

*Work performed under auspices of the U.S. D.O.E. by the University of California, Lawrence Livermore National Laboratory under Contract No. W-7405-ENG-48.

The equations solved at each node are:

$$C_i \frac{dV_{i+1}}{dt} = I_i - I_{i+1} + I_{b,i} - I_{b,i+1} \tag{1}$$

$$L_i \frac{dI_i}{dt} = V_i - V_{i+1} \tag{2}$$

Here, Eq. 1 relates the current that flows through the capacitances to ground (that is, the difference between the currents through neighboring inductors) to the voltage drop across those capacitances. Eq. 2 describes the usual relationship between the current (I_i) through and the voltage drop ($V_i - V_{i+1}$) across each inductor i. In all examples considered to date, the component values are independent of the index i. The quantities in the left members of these equations are temporally advanced through a time step Δt using a "split leapfrog" advance similar to that used in the WARP code for advancing particles; the splitting allows key quantities to all be defined at integer time levels, aiding clarity and the implementation of diagnostics. The sequence is: a half-step current advance (Eq. 2) using the V values at the old time level in the right member, and discretizing the time derivative across an increment $\Delta t/2$; a full-step voltage advance Eq. 1 with a centered time difference across the full Δt; and finally a second a half-step current advance to bring the I values to the "future" time level.

The beam current I_b is accompanied by a return current that flows through the helix and (because of the capacitive coupling) the wall. It enters as a time-varying surface charge that induces a voltage on the node via the capacitance. To see this, note that in the continuum limit (all quantities varying smoothly with time and axial coordinate z) Eq. 1 becomes:

$$\frac{\partial I}{\partial z} = -\mathcal{C}\frac{\partial V}{\partial t} - \frac{\partial I_b}{\partial z} = -\mathcal{C}\frac{\partial V}{\partial t} + \frac{\partial \lambda_b}{\partial t} \tag{3}$$

where $\mathcal{C}$ is the capacitance per unit length, λ_b is the beam line charge density, and the latter equality follows from the continuity equation. Similarly, Eq. 2 becomes:

$$\frac{\partial V}{\partial z} = -\mathcal{L}\frac{\partial I}{\partial t}\ , \tag{4}$$

where $\mathcal{L}$ is the inductance per unit length. Combining these two equations yields a wave equation; the pulse-line's circuit speed (wave speed) is $v_c = (\mathcal{L}\mathcal{C})^{-1/2}$.

To quantify the uniformity of the acceleration, the positions and velocities of a set of marker (test) particles are advanced in time along with the circuit quantities. At present these particles carry no current, and serve primarily as a diagnostic. However, in studies of beam loading effects the (assumed) current profile is made to move down the beamline in such a way that the current peak tracks the center-of-mass of the marker particles; this affords a measure of the beam slowing due to return current loading effects. Thus at this point in time the model is *not* fully self-consistent. The current pulse retains its initially-imposed profile, and space-charge effects are not included. Nonetheless, when the beam loading effects are small, the method yields useful information about the dependence of those effects upon the beam current. The largest space-charge effects (especially pulse expansion) will be controlled by shaping the accelerating waveforms; separate studies using WARP are quantifying the requirements for this.

2 A low-current acceleration example

No attempt was made to capture exactly the parameters of the planned experiment; rather, the parameters were chosen to afford a "clean" example of the acceleration of a bunch that is significantly shorter than the voltage ramp. The inductance and capacitance were chosen to yield a wave speed in the range being considered for the experiments, and roughly correspond to the self-inductance of a single turn of the helix and the capacitance between that turn and the grounded outer wall.

In this run, the accelerating pulse is omitted, and a prescribed beam sent down the pulse-line and allowed to induce a voltage profile on the nodes. Key parameters for these runs are: $n = 320$ nodes, $s = 3$ mm, $L_i = 0.3$ μH, $C_i = 3.33$ pF, $R_{\text{final}} = 300$ Ω (terminating resistor matched to pulse-line impedance), timestep size $\Delta t = 0.01$ ns, $m_{\text{ion}} = 39$ amu. The circuit speed $v_c = 3$ m/μs.

The accelerating pulse has the "smooth linear" profile:

$$V_1(t) = V_0 \frac{t - t_{\text{offset}}}{t_{\text{main}}} \exp - \left[\frac{t - t_{\text{offset}}}{t_{\text{main}}} \right]^{N_V} \tag{5}$$

and for the run described here, $V_0 = 200$ kV, the exponent $N_V = 4$, $t_{\text{offset}} = 100$ ns, and $t_{\text{main}} = 50$ ns. The marker particles are injected every $\Delta t_{\text{inject}} = 1$ ns beginning at time t_{inject} after the run begins, and continue to be injected over the interval τ_{pulse}. If the beam were to travel at constant speed, it would be centered at

$$\bar{z} = v_{\text{inject}} \left[t - (t_{\text{inject}} + \tau_{\text{pulse}}/2) \right],$$

where in this case $v_{\text{inject}} = 2.3$ m/μs, $t_{\text{inject}} = 75$ ns, and $\tau_{\text{pulse}} = 15$ ns. This applied voltage $V_1(t)$ is shown in Fig. 2.

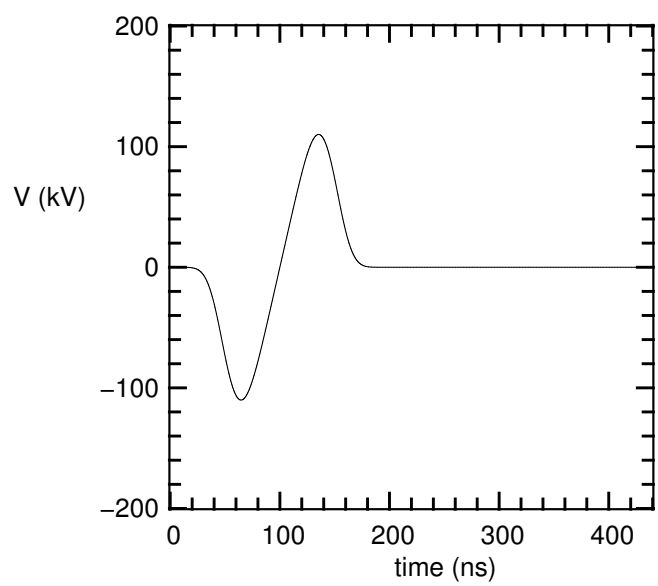

Figure 2: Applied voltage profile $V_1(t)$.

The profiles of the electric field, and the locations of the marker particles, are shown at a set of equally-spaced times during the run; see Fig. 3. Note that the abscissa in these plots is a "moving window" in z. The beam falls back relative to the wave, but as it does so it gains sufficient energy

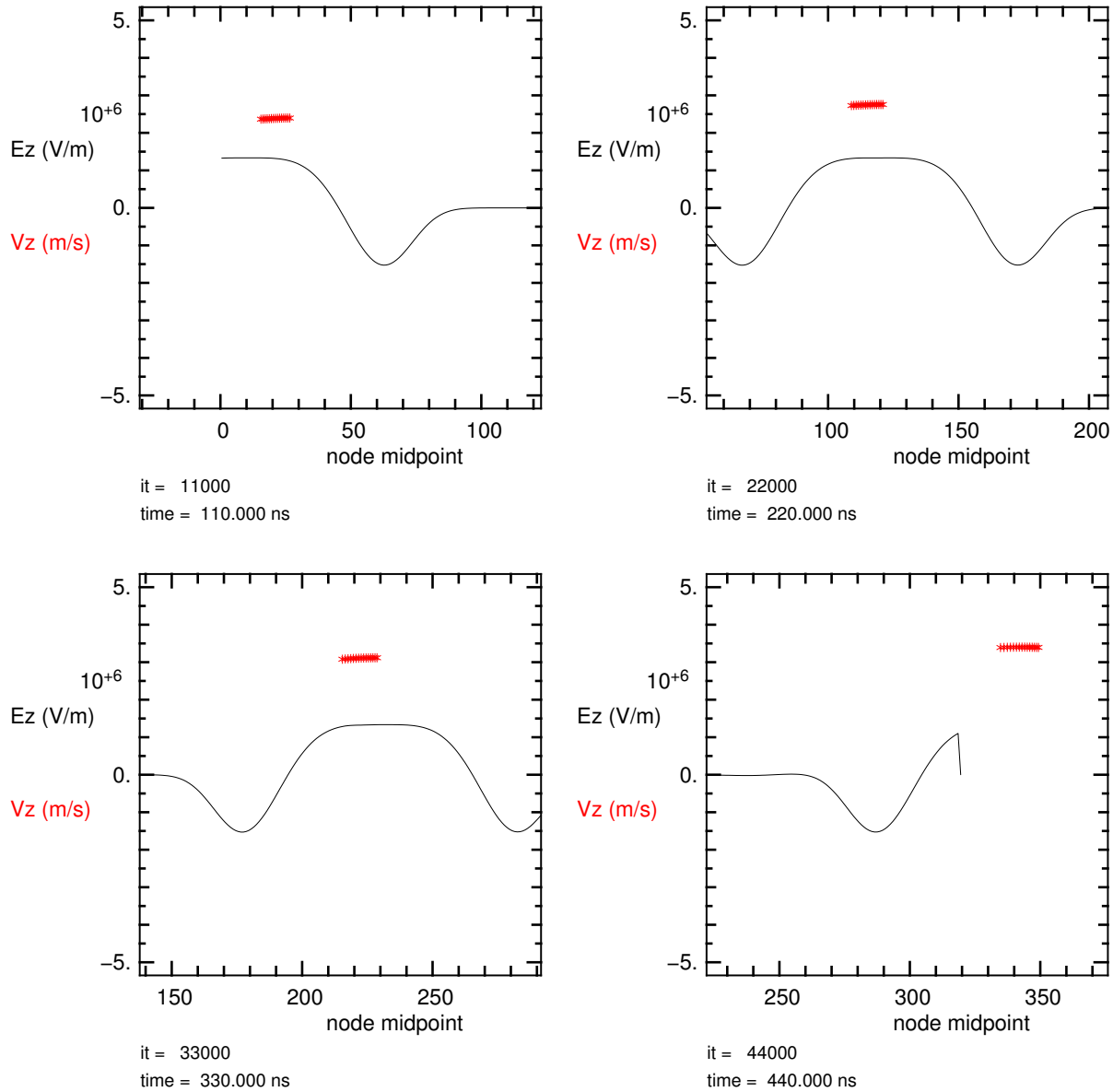

Figure 3: Electric field and marker particles for 20 mA run.

that it begins to run forward (in the wave frame) before it reaches the tail end of the accelerating field. At the end of the run, the beam has run past the end of the helix, and is free-streaming. The mean particle velocity has increased from 2.3 to 3.398 m/μs and the kinetic energy from 1.069 to 2.334 MeV, with a final relative spread of the marker particle speeds $v_{\rm thermal}/\bar{v} = 9.59 \times 10^{-4}$ (this spread is not really "thermal," since no overtaking has occurred and the marker velocities are unique at each z). Achieving this small a spread required adjustment of the relative timing of the particle and wave injection (perhaps half a dozen iterations by hand). To date, this code has not yet been used for sensitivity studies to quantify the tolerances on timing, waveform shape and amplitude, and other factors, though such studies are planned.

3 Beam loading of the circuit

For these runs the drive voltage $V_1(t)$ is zero; see Fig. 4. We consider first a Gaussian current pulse injected with initial speed v_{inject} equal to the circuit speed v_c. The spatial variation is:

$$I_b(z) = I_{b0}\ \exp - \left[\frac{z - \bar{z}}{v_{\text{inject}}\tau_{\text{pulse}}/2}\right]^2 \tag{6}$$

where the peak current $I_{b0} = 20$ mA and other parameters are as described in the previous section. The marker particles are also injected as described in the preceding section; the current pulse span roughly the same interval as the markers, but has the user-specified profile $I_b(z)$ while the markers are distributed uniformly.

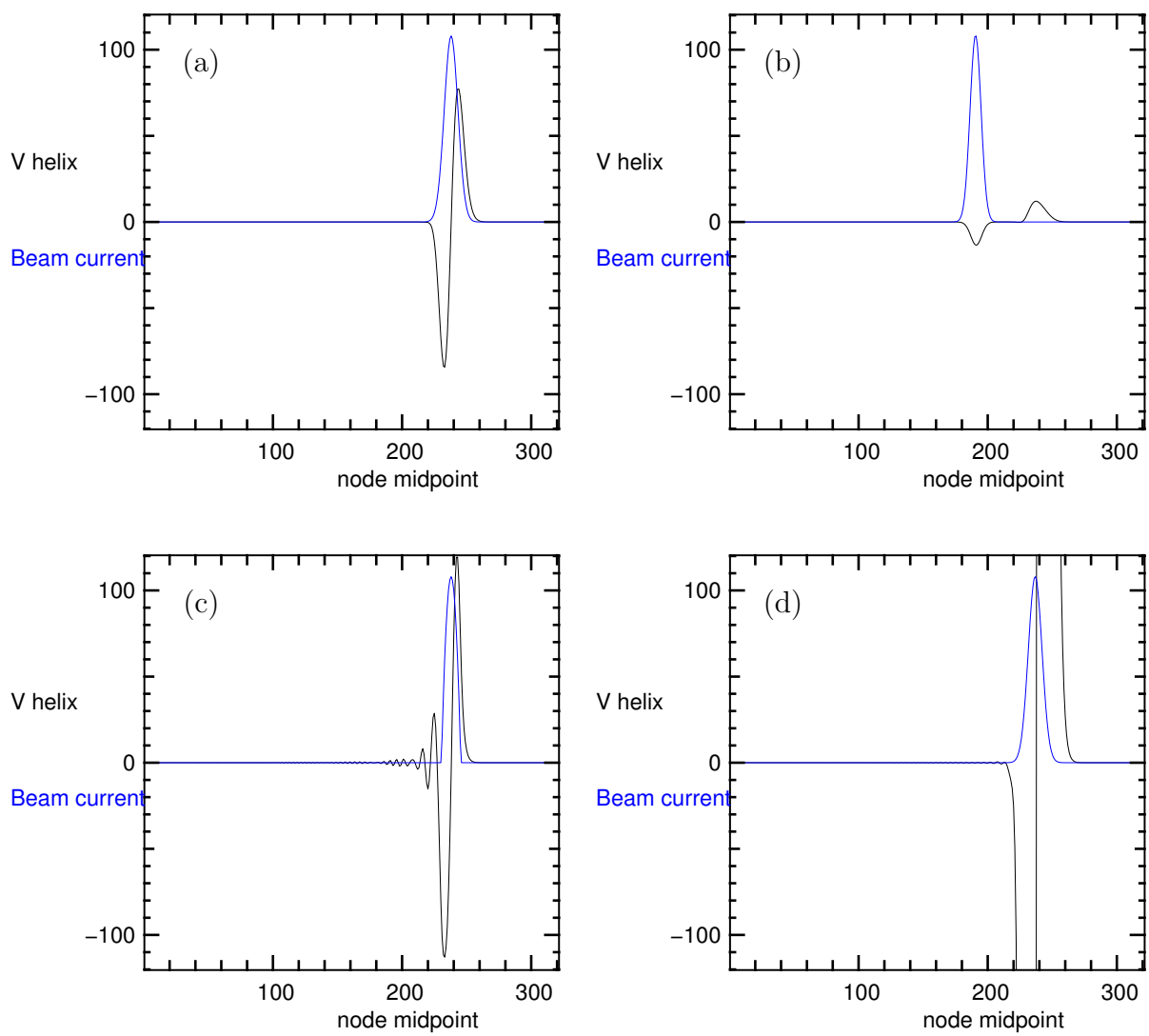

Figure 4: Beam current (arbitrary units) and induced voltage after 320 ns, for (a) 20 mA Gaussian-profile case with $v_{\text{inject}} = v_c$; (b) 20 mA Gaussian-profile case with $v_{\text{inject}} = 0.8v_c$; (c) 20 mA parabolic-profile case with $v_{\text{inject}} = v_c$; and (d) 1 A Gaussian-profile case with $v_{\text{inject}} = v_c$; the induced voltage has gone far off-scale.

The current and voltage waveforms after the beam has traveled some distance are shown in Fig. 4(a). As predicted by the analysis by Briggs, the effect of the loading is to induce a retarding force over the main body of the beam. In this case, the loading is so small as to induce negligible slowing.

In a second example, the parameters are unchanged except that $v_{\text{inject}} = 0.8v_c$. In this case, shown in Fig. 4(b), features traveling at both the circuit (wave) speed and the particle speed are evident; the amplitude of the induced voltage is considerably reduced. In the actual system, under most scenarios the beam does not travel synchronously at the wave speed, and so synchronous motion may be used as a worst-case estimator.

A third example is identical to the first except that a parabolic pulse is used, with spatial variation:

$$I_b(z) = \max\left\{ I_{b0}\left[1 - \left(\frac{z-\bar{z}}{v_{\text{inject}}\tau_{\text{pulse}}/2}\right)^2\right],\ 0\right\} \tag{7}$$

and in this case, shown in Fig. 4(c), the retarding force affects (almost) the entire beam, also as derived by Briggs. Note the presence of oscillations associated with the sudden turn-on of this waveform and the dispersion at short wavelengths resulting from the discreteness of this model.

In the fourth and final example of this section, the parameters were the same as in the first example, except that the beam current was increased to 1 Ampere. This larger current induces a voltage sufficient to cause noticeable slowing of the beam, from 3 m/μs to 2.953 m/μs over the course of the run. See Fig. 4(d). A similar run with a parabolic beam showed somewhat more slowing, to 2.937 m/μs. In both of these cases, the slowing is slight enough that the *ansatz* of the beam's retaining its profile seems justified; indeed, it was probably unnecessary to force the current centroid to track the center-of-mass of the marker particles.

4 A higher-current acceleration example

A run was made with parameters identical to those of the run described in Sec. 2, except that the beam current was raised to 1 Ampere. Results from this latter run are shown in Fig. 5. The mean particle velocity has increased from 2.3 to 3.349 m/μs and the kinetic energy from 1.069 to 2.267 MeV, with a final relative spread of the marker particle speeds $v_{\text{thermal}}/\bar{v} = 7.997 \times 10^{-3}$. This lower final velocity and energy (relative to the low-current run's values of 3.398 m/μs and 2.334 MeV) is a consequence of the beam loading. The larger velocity spread is in part due to the distortion of the traveling wave by the non-constant beam loading, and in part because the timing is no longer near-optimal. Even at this current, no marker overtaking has taken place. However, the separation between the first and the last marker particle has changed from 0.033 m to 0.031 m, the RMS of the marker z values has changed from 0.0102 m to 0.0082 m, and the markers are now no longer distributed uniformly in z by the end of the run (see Fig. 6). Thus, the constancy of the current profile assumed in this simple version of the code is not quite correct. Nonetheless, it appears that even at this large current, which is far higher than envisioned for near-term experiments, the effects of beam loading are likely to be modest.

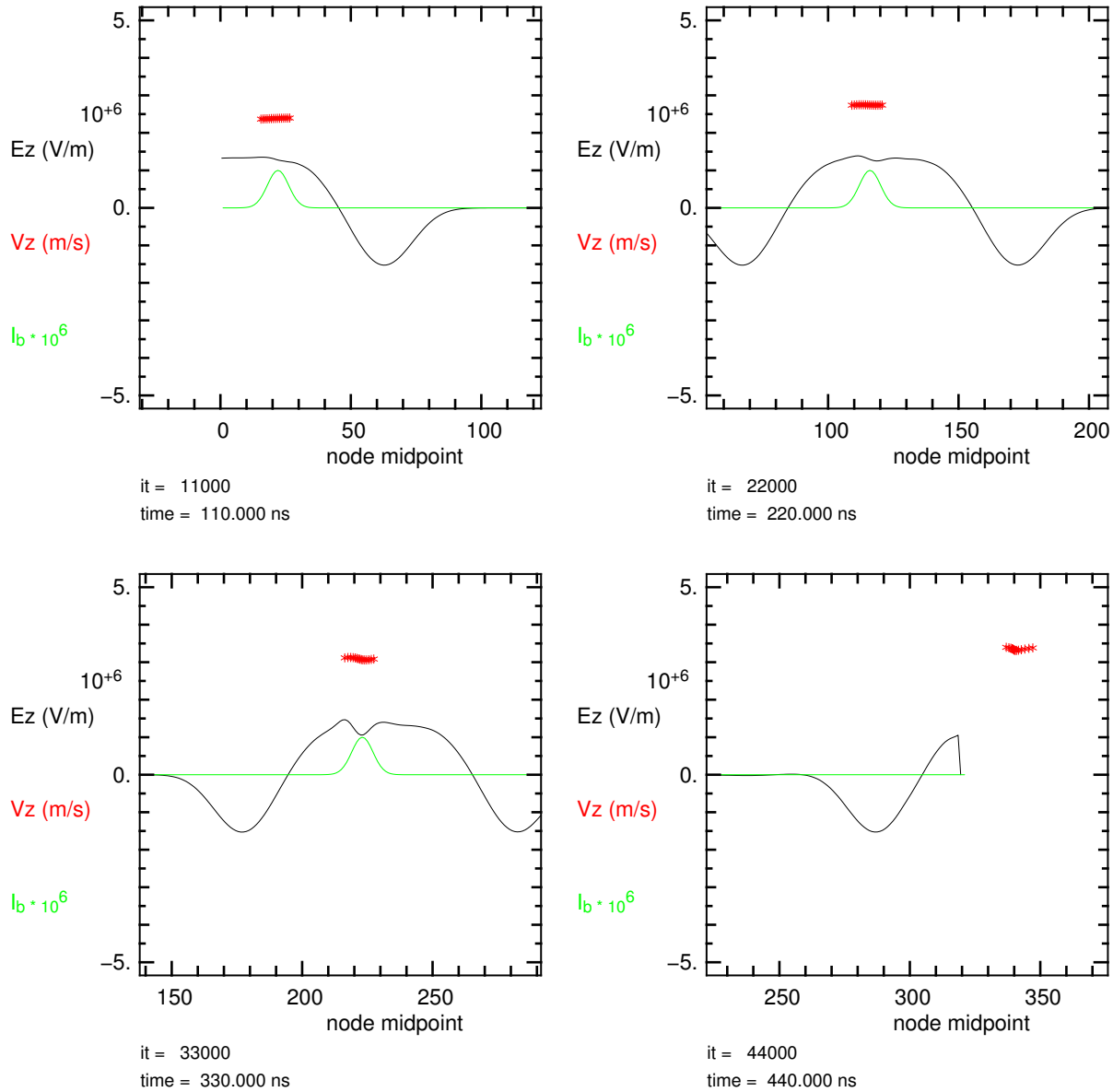

Figure 5: Electric field, marker particles, and beam current profile (as modeled) for 1 A run.

5 Discussion and plans

This modeling represents only a fraction of the work being carried out using analysis, simulation, and bench testing to understand this novel approach to ion acceleration. The analyses by R. J. Briggs and G. J. Caporaso have laid (and continue to clarify) the basic groundwork for the concept. Computer simulations of electromagnetic pulse propagation by S. Nelson from "first principles," using a three-dimensional finite-difference time-domain code, are lending valuable insight into the spatial structure of the field, the pulse dispersion (in an initial-value sense), and the magnitude of transverse fields associated with the helical symmetry of the coil. Particle-in-cell simulations using the WARP code by D. P. Grote and E. Henestroza (mostly in (r, z) geometry so far, though 3D runs are planned) are exploring the effects of transverse and longitudinal space charge forces in realistic solenoid fields, using (so far) idealized accelerating waveforms shaped to confine the beam. WARP

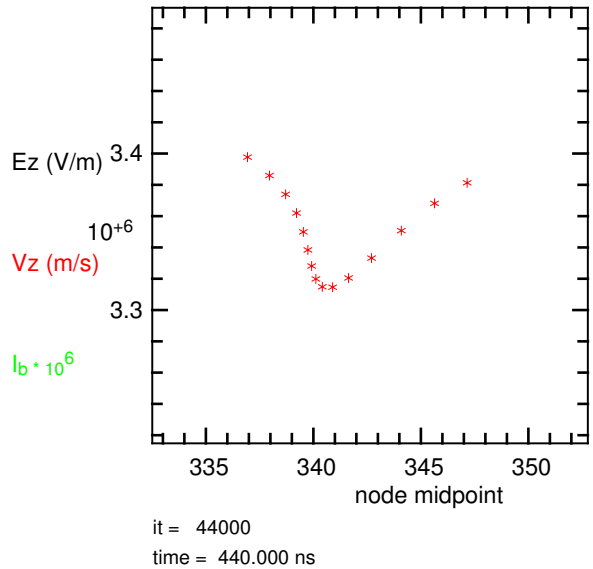

Figure 6: Marker particles (expanded view) at end of 1 A run.

runs are exploring both the "normal" pulse-line accelerating regime and a "snowplow" mode, which is an alternative to the resistively-graded line used for initial load-and-fire launching of the beam after it emerges from the emitting region. Analysis of some advanced concepts by B. G. Logan have helped delineate some applications of the concept. Finally, bench tests by W. Waldron, R. J. Briggs, and L. Reginato have shown that the waves do indeed propagate as expected, and serve as "analog models" of the lines to be used on the NDCX apparatus.

Improvements to the model described herein are planned. The injection of the particles which now serve as markers will be generalized so that their injection rate at any instant is proportional to the entering beam current at that instant; then the current $I_b(z,t)$ will be computed from the marker particles via a particle-in-cell deposition (with linear weighting to the two nearest nodes). This will allow study of the small-signal behavior of the traveling-wave-tube mode of instability, as an initial value problem in a fully causal way. (Analysis of that mode in this context is already underway by R. J. Briggs).

Improvements to the circuit description will also be implemented. The goal will be to improve the dispersion so that the wavenumber-dependent $\mathcal{L}(k)$ and $\mathcal{C}(k)$ are properly captured. However, we do not want to work in the transformed space because it will be important to faithfully model the wave behavior near the two ends of the pulse line. Thus we will develop expressions for the mutual inductances M_{ij} and capacitances C_{ij} that in a periodic system yield the correct wavenumber dependence. This may be validated by running the small code with a drive voltage that is harmonic in time (with no marker particles or return current feedback) and measuring the spatial wave spectrum along the nodes. Benchmarking the code versus the small helices being measured in the laboratory is planned; the experimental data are not sufficiently complete to fully specify the model, but are complete enough to serve as valuable checks.

It had been hoped that it would prove possible to run this model with a fundamental node spacing longer than a single turn of the helix, to allow M_{ij} and C_{ij} to be narrowly banded or even tridiagonal. However, a test with the node spacing (and the L and C values) increased by a factor of four showed greater short-wavelength dispersion; for the 20 mA acceleration case, the final relative velocity

spread was 2.25×10^{-3}, larger by a factor of roughly three than in the reference case (some of this might be removable by re-tuning). Most of the extra ripple appeared late in the run, and seemed to be associated with end effects. The calculations of Nelson suggest the existence of considerable short-wavelength smoothing in the real system—sharp transitions in the applied waveforms do not seem to lead to ringing in his runs, while they do in these circuit calculations, as also seen for the parabolic current test described above. In any event, once the M_{ij} and C_{ij} have been approximately set, comparisons will be made with Nelson's runs and the model tuned iteratively.

The effects of space charge are not included in this small code. In a real beam, waves propagate longitudinally, with dispersion governed by a combination of electrostatic and thermal forces. In the case of an induction accelerator, space-charge wave propagation has been shown to render the unstable "resistive wall" modes convective in nature, with a single pass of head-to-tail growth of the unstable branch. Also, self-consistent accelerating scenarios can only be captured when space charge is included, because the driving wave shape must be altered to counteract the space-charge repulsion. Thus, it will be important to incorporate space-charge physics. However, this small code was written in an interpretive language (Yorick) and considerable effort would be required to implement an (r, z) particle-in-cell model using compiled code to obtain the necessary computational speed. Simpler 1D kinetic models are possible, using an expression for $E_z \propto -\partial\lambda_b/\partial z$, but these have proven problematic for beams which do not vary quite slowly in z. Thus for high fidelity we plan to handle space-charge effects in WARP, with improved models as described below.

Plans for WARP modeling will follow two branches. S. Nelson is exporting the field data from his calculations, and WARP can import that data and use those fields (in addition to the space-charge forces computed by WARP itself) to advance the simulation particles. It may be most valuable to tabulate the response of a given helix (with associated drive coupling and termination) to a unit impulse of applied voltage (the voltage is applied either to the helix itself or to the primary of a transformer coupler). Then WARP can run with any applied waveform by summing suitable scaled and time-shifted impulses.

The second branch of WARP model development will consist of the implementation of this circuit model (once it has been refined, as described above) directly into WARP. By deriving voltages at nodes along the wall and using them as boundary conditions for Poisson's equation, the Bessel function falloff of short wavelength modes toward the axis will automatically be captured. In addition, the coupling from the beam back onto the circuit (return current driven beam loading) will also be smoothed, since the image charge in the cylindrical wall for each simulated ion is "smeared" in z. In applications where the efficiency of the accelerator is important (such as inertial fusion energy), the beam loading must be significant, and this feedback must be handled correctly.

Despite its simplicity, this model has already provided valuable insights into the physics of pulse-line ion acceleration, and lends confidence to analytical calculations of such effects as beam loading and mismatch between ion and wave speeds. It seems likely to remain a useful exploratory tool even after more complete descriptions have been developed.

References

[1] See the relevant sections (available upon request) of the Proceedings of the Workshop on Accelerator Driven High Energy Density Physics, LBNL, October 26-29, 2004; also patent application by R. Briggs.